Vol. 92 No. 2 pp. 786–800 ACTA GEOLOGICA SINICA (English Edition) Apr. 2018

^{10}Be Exposure Ages Obtained From Quaternary Glacial Landforms on the Tibetan Plateau and in the Surrounding Area

ZHANG Mengyuan[1, 2, 3], MEI Jing[1, 2, 3], ZHANG Zhigang[1, 2, 3, 4, *], WANG Jian[1, 2, 3] and XU Xiaobin[5]

1 *School of Geographical Sciences, Nanjing Normal University, Nanjing 210023, China*
2 *Key Laboratory of Virtual Geographic Environment (Nanjing Normal University), Ministry of Education, Nanjing 210023, China*
3 *Jiangsu Center for Collaborative Innovation in Geographical Information Resource Development and Application, Nanjing 210023, China*
4 *State Key Laboratory of Cryospheric Sciences, Northwest Institute of Eco-Environment and Resources, Chinese Academy of Sciences, Lanzhou 730000, China*
5 *School of Urban and Resource Environment, Jiangsu Second Normal University, Nanjing 210024, China*

Abstract: In situ terrestrial cosmogenic nuclide (TCN) exposure dating using ^{10}Be is one of the most successful techniques used to determine the ages of Quaternary deposits and yields data that enable the reconstruction of the Quaternary glacial history of the Tibetan Plateau and the surrounding mountain ranges. Statistical analysis of TCN ^{10}Be exposure ages, helps to reconstruct the history of glacial fluctuations and past climate changes on the Tibetan Plateau, differences in the timing of glacier advances among different regions. However, different versions of the Cosmic-Ray-prOduced NUclide Systematics on Earth (CRONUS-Earth) online calculator, which calculates and corrects the TCN ages of Quaternary glacial landforms, yield different results. For convenience in establishing contrasts among regions, in this paper, we recalculate 1848 ^{10}Be exposure ages from the Tibetan Plateau that were published from 1999 to 2017 using version 2.3 of the CRONUS-Earth calculator. We also compare the results obtained for 1594 ^{10}Be exposure ages using different versions (2.2, 2.3 and 3.0) of the CRONUS-Earth calculator. The results are as follows. (1) Approximately 97% of the exposure ages are less than 200 ka. A probability density curve of the exposure ages suggests that greater numbers of oscillations emerge during the Holocene, and the peaks correspond to the Little Ice Age, the 8.2 ka and 9.3 ka cold events; the main peak covers the period between 12 and 18 ka. (2) In most areas, the newer versions of the calculator produce older ^{10}Be exposure ages. When different versions of the CRONUS-Earth calculator are used, approximately 29% of the ^{10}Be exposure ages display maximum differences greater than 10 ka, and the maximum age difference for a single sample is 181.1 ka.

Key words: ^{10}Be, probability density curves, in situ terrestrial cosmogenic nuclides, CRONUS-Earth, Tibetan Plateau

1 Introduction

Most modern glaciers, except for those located in the polar regions, are located on the Tibetan Plateau; the Tibetan Plateau also displays the largest number of developmental stages of Quaternary glaciers, and the largest number of preserved ancient glacial relics is found there (Dyurgerov and Meier, 2005; Zhao Jingdong et al., 2009; Owen and Dortch, 2014; Yao Tandong et al., 2017). Studying the temporal and spatial changes in the glaciers on the Tibetan Plateau during the Quaternary is of great significance in paleo-environmental reconstructions and increasing our understanding of environmental changes on the hemispheric and even global scales (Heyman et al., 2011b; Wang Jian et al., 2012). As the in situ terrestrial cosmogenic nuclide (TCN) dating method has been developed (Dyke et al., 2002; Zhou Shangzhe and Li Jijun, 2003), it has become one of the most successful techniques used to determine the ages of Quaternary glacial landforms (Wu Zhonghai et al., 2003; Kong et al.,

* Corresponding author. E-mail: zhangzhigang840620@126.com

2009a; Owen, 2009b; Li et al., 2011; Zhang et al., 2014c, 2015). TCN surface exposure dating enables reconstruction of the Quaternary history of glacial fluctuations and reveals the characteristics of climate changes on the Tibetan Plateau and in the adjacent areas (Wang Jie and Zhou Shangzhe, 2009; Heyman et al., 2011b; Heyman, 2014; Owen et al., 2012; Owen and Dortch, 2014; Wang et al., 2013).

However, due to the effects of the geological and geomorphological characteristics of sampling sites and dating techniques (Lal, 1991; Gosse and Phillips, 2001; Briner et al., 2005; Zech et al., 2005b), TCN surface exposure dating includes substantial uncertainties. Complex geological and geomorphological processes, sampling and post-processing procedures and surface erosion rates affect the accuracy of TCN surface exposure dating (Owen, 2009b; Zhao Jingdong et al., 2013; Zhang Zhigang et al., 2014a; Xin Chunlei, 2016). Furthermore, as the Cosmic-Ray prOduced NUclide Systematics on Earth (CRONUS-Earth) online calculator is progressively updated, the differences among versions of the calculator also affect the dating results. These differences lead to controversies in comparisons of reconstructions of the chronology of the Quaternary history of glacial fluctuations on the Tibetan Plateau and the glacial advances in different regions. Therefore, it is very important to unify all of the ^{10}Be dating results obtained from the different regions on the Tibetan Plateau. Many scholars have summarized the chronological data obtained from glacial landforms on the Tibetan Plateau (Chevalier et al., 2011; Heyman, 2014; Owen and Dortch, 2014). The CRONUS-Earth online calculator (http://hess.ess.washington.edu) can be used to calculate cosmogenic nuclide surface exposure ages. Previously, scholars employed version 2.2 of the CRONUS-Earth calculator to calculate TCN exposure ages. As this version has been updated, it has become necessary to use more accurate and stable versions of the calculator to recalculate previous TCN data (Borchers et al., 2016; Marrero et al., 2016; Balco, 2017). In addition, different versions of the CRONUS-Earth calculator yield different results for the same sample. Assessing these differences and their effects on the TCN surface exposure ages is key in establishing an accurate chronology of the history of glacial fluctuations on the Tibetan Plateau. Accordingly, this article examines the impact of different versions of the CRONUS-Earth calculator on the exposure ages obtained from Quaternary glacial landforms on the Tibetan Plateau and within the surrounding area using the TCN ^{10}Be from 1999 to 2017 and explores some existing problems. This research will provide a new reference for the application of the TCN surface exposure dating method in the establishment of accurate chronological frameworks for the history of glacial fluctuations.

2 Study Area and Data Collection

The Tibetan Plateau is called “the roof of the world” and “the third pole”, which caused by the Indian-Eruasian continental collision since 50 million years ago, forms the youngest and highest altitude Plateau on Earth. A large number of geophysical and geological surveys have found that the major tectonic features of the Tibetan Plateau show a significant difference between north and south directions, and is divided into several terranes by faults and suture (Fig. 1). (Shi Yafeng et al., 1999a; Kind et al., 2002; Zheng Du and Yao Tandong, 2004; Zhou et al., 2005; Li et al., 2016a; Tang et al., 2016; Zhang et al., 2016). The Tibetan Plateau stretches from the Himalayan Mountains in the south to the Kunlun, Altun and Qilian Mountains in the north and from the Pamirs and the Hindu Kush to the west to the western part of the Qinling Mountains and the Loess Plateau to the east and northeast. The average altitude of the Tibetan Plateau is over 4000 m, and its glacier-covered area is approximately 47 thousand km^2, which accounts for more than 80% of the total area of glaciers in the country. The Tibetan Plateau contains the largest extent of modern glaciers outside of the polar regions (Owen and Dortch, 2014; Yao Tandong et al., 2017; Chen Guohui and Ma Ling, 2017). For this study, we collected 1848 ^{10}Be ages obtained from the Tibetan Plateau and the peripheral mountain ranges published from 1999 to 2017 in 56 articles. We extracted the information relevant to TCN exposure dating for the sampling locations (latitude, longitude, altitude, altitude flag, sample thickness and density, shielding correction and erosion) and the measured parameters (concentration of ^{10}Be, uncertainty in ^{10}Be concentration, and name of ^{10}Be standardization). The distributions of these data are shown in Figure 2. The data were collected within an area that extends from 27.04°N to 43.74°N and from 69.50°E to 102.74°E; the corresponding study areas (1–36) are shown in Table 1. Most (1798; approximately 97.3%) of the samples were collected from boulders; samples from cobbles (22; approximately 0.8%), bedrock (15; approximately 1.2%), roches moutonnées (7; approximately 0.4%) and sediments (6; approximately 0.3%) make up a small part of the dataset.

3 Methods

3.1 Calculation of ^{10}Be exposure ages using different versions of the calculator

The CRONUS-Earth online calculator (http://

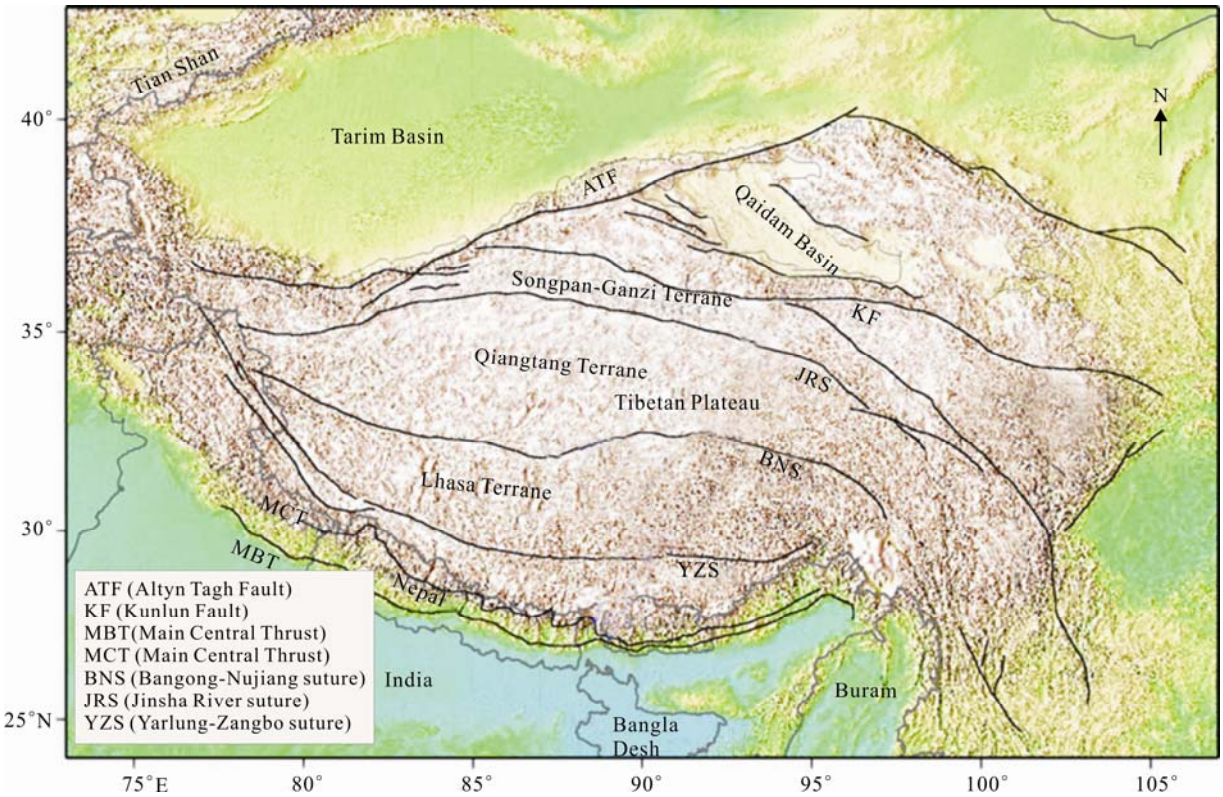

Fig. 1. Topographic map of Tibetan Plateau and surrounding areas (modified from Kind et al., 2002).

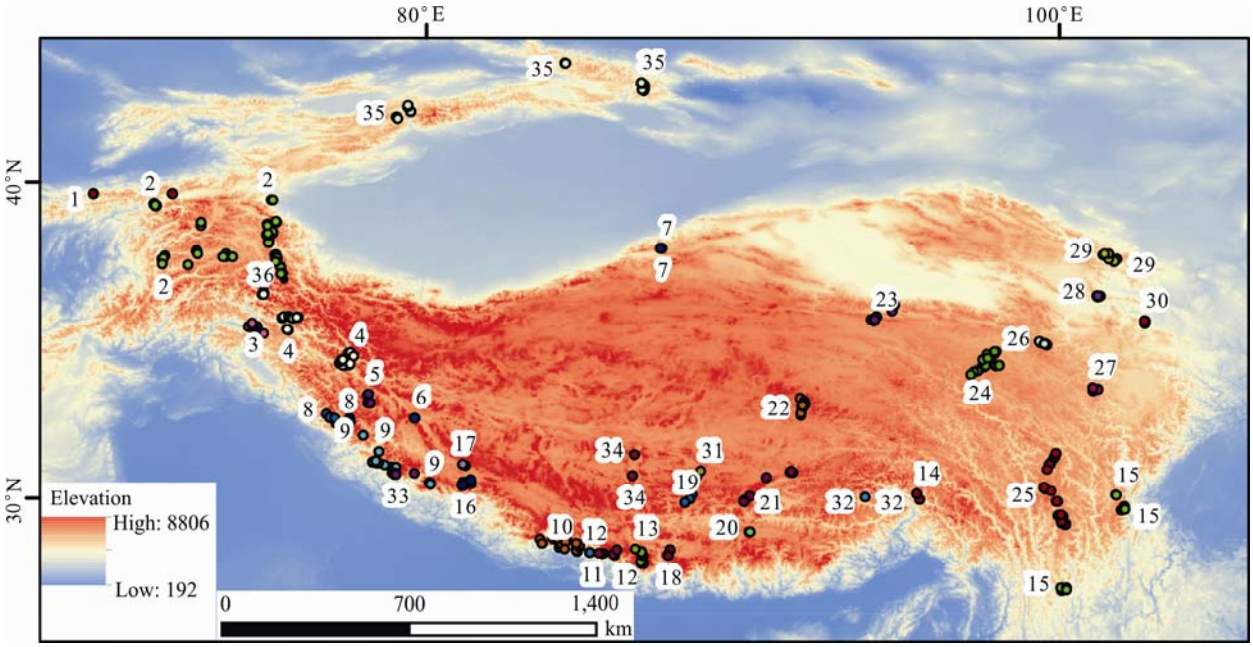

Fig. 2. The location of published TCN ^{10}Be exposure age studies of Tibetan Plateau (modified from Wang et al., 2013).

hess.ess.washington.edu) computes exposure ages (Balco et al., 2008). According to the naming scheme used by the developer, the original online calculator is called 2008-V2. However, some of the parameter values used in this version are inaccurate, which will have a significant impact on exposure dating. A revised and improved version, 2008-V2.2 (here called version 2.2), was published in 2009 and was in use until August 2016. CRONUS-2016 was subsequently developed. This version of the calculator incorporates seven different production rate scaling models and uses more complex and accurate representations of physical processes and is thus more accurate than previous versions (Marrero et al., 2016). Nevertheless, users still have considerable demand for

Table 1 Information of TCN ^{10}Be exposure ages studies of Tibetan Plateau

No	study region	publication	No	study region	publication	No	study region	publication
1	Alay Mount Turestan Range	Abramowski et al., 2006	13	Everest	Aoki and Imamura, 1999; Finkel et al., 2003; Owen et al., 2009a; Chevalier et al., 2011	25	Shaluli Shan	Schäfer, 2000, Schäfer et al., 2002; Wang et al., 2006; Graf et al., 2008; Fu et al., 2013
2	Pamirs Mount	Zech et al., 2005a; Abramowski et al., 2006; Seong et al., 2009; Owen et al., 2012; Grin et al., 2016; Stübner et al., 2017	14	Bodui Zangbo River	Zhou et al., 2007, 2010	26	Anyemaqen	Owen et al., 2003a
3	Naga Parbet	Phillips et al., 2000	15	Hengduan Mount	Tschudi et al., 2003; Owen et al., 2005; Kong et al., 2009b; Strasky et al., 2009	27	Nianbaoyeze	Owen et al., 2003a
4	Karakoram and Ladakh Range	Brown et al., 2002; Owen et al., 2002, 2006a; Seong et al., 2007; Dortch et al., 2010	16	Gular Mandhata	Owen et al.,2010; Chevalier et al., 2011	28	Laji Mount	Owen et al., 2003b
5	Zanskar Range	Hedrick et al., 2011	17	Kailas Range	Chevalier et al., 2011	29	Qilian Mount	Lasserre et al.,2002; Owen et al., 2003c
6	Ayliari Range	Chevalier et al., 2011	18	Ama Drime Range	Chevalier et al., 2011	30	Dalijia Shan	Wang et al., 2013
7	Altyn Mount	Mériaux et al., 2004	19	Xainza Range	Chevalier et al., 2011	31	Mount Jaggang	Dong et al., 2017a
8	Lahul Himalayas	Owen et al., 2001	20	Karola Pass	Owen et al., 2005	32	Eastern Himalayan syntaxis	Hu et al., 2016
9	Garhwal Himalayas and Bandarunch Range	Barnard et al., 2004; Scherler et al., 2010	21	Nyainqentanggula	Owen et al., 2005; Chevalier et al., 2011; Dong et al., 2014, 2017b	33	Himalayane Tibetan orogen	Murari et al., 2014
10	Annapurna Range	Abramowski, 2004; Pratt-Sitaula, 2005; Zech et al., 2009	22	Tanggula Shan	Schäfer et al., 2002; Owen et al., 2005; Colgan et al., 2006	34	South Tibetan graben	Rades et al., 2015
11	Ganesh Himalayas	Gayer et al., 2006	23	Eastern Kunlun Mount	Owen et al., 2006b	35	Tian Shan Mount	Li et al., 2014; Lifton et al., 2014; Li et al., 2016b
12	Langtang Himalayas	Abramowski, 2004; Barnard et al., 2006; Schaefer et al., 2008	24	Bayan Har Shan	Heyman et al., 2011b	36	Tashkurgan Valley	Xu et al., 2013

version 2.2, and 2008-V2.3 (here called version 2.3) was thus developed. In most practical applications, V2.3 displays the same level of accuracy as CRONUS-2016 in calculating exposure ages (Borchers et al., 2016). In March 2017, the latest version of the online calculator (version 3.0), was published to permit more rapid calculations of exposure ages. While it maintains acceptable accuracy, its accuracy and reliability have not been widely tested (Balco, 2017). Therefore, in this paper, version 2.3 of the CRONUS-Earth calculator (effective August 2016), which is relatively accurate and stable, is used to recalculate previously published ^{10}Be ages of glacial landforms on the Tibetan Plateau. Moreover, the ^{10}Be exposure ages of 1594 samples are calculated using three different versions of the calculator, 2.2, 2.3 and 3.0, to enable comparison of the differences that result. The exposure ages calculated using version 2.0 are derived from the work of Zhang Zhigang et al. (2014b) (Now, version 2.2 has been removed from http:// hess.ess.washington.edu), whereas versions 2.3 and 3.0 of the calculator are available online. To compare the differences in the exposure ages calculated using the three different versions of the calculator more accurately; the production rate model of Lal (1991) and Stone (2000) is used to calculate the ages.

3.2 Calculation of the dispersion of ^{10}Be exposure ages

The exposure ages obtained using different versions of the CRONUS-Earth calculator for a single sample (for which the sampling environment and the measured parameters of the sample remain unchanged) vary, due to the continuous updating of the calculator by its developers. This article uses the coefficient of variation to explore the dispersion among the exposure ages calculated for individual samples using versions 2.2, 2.3, and 3.0 of the calculator. The coefficient of variation is a dimensionless quantity whose size is affected by the mean and standard deviation. A small coefficient of variation indicates that the data display little spread, whereas a large coefficient of variation indicates that the data are widely

dispersed. Under normal circumstances, a coefficient of variation greater than 1 indicates strong variation; a coefficient of variation between 0.1 to 1 indicates moderate variation; and a coefficient of variation less than 0.1 indicates weak variation (Yonker et al., 1998). The formula is as follows (Cressie, 1992):

$$C.V = \frac{\sigma}{\mu}$$

where $C.V$ is the coefficient of variation, σ is the sample standard deviation, and μ is the sample mean.

In addition, this paper also uses box plots and probability density curves to analyze the ^{10}Be exposure ages.

4 Results

4.1 TCN dating results

Because version 2.3 is relatively accurate and stable, 1848 ^{10}Be exposure ages are recalculated using version 2.3, and the statistical results are shown in Table 2. Approximately 93% of the exposure ages are less than 130 ka, whereas approximately 97% of the chronological data are less than 200 ka. According to the method adopted by Wang et al. (2013), the study area is divided into 36 different areas (Fig. 2). The distribution of ^{10}Be exposure ages in different areas is shown in Figure 3.

To further determine the possible timing of glacier advances and retreats on the Tibetan Plateau and in its peripheral mountain ranges, the 1848 ^{10}Be ages are analyzed using probability density curves. The results are shown in Figure 4. As seen in Figure 4a, the probability density curves display large numbers of local minima during the Holocene, and the peak values correspond to the Little Ice Age and the 8.2 ka and 9.3 ka cold events. Figure 4b does not display a primary peak corresponding to the Last Glacial Maximum (approximately 21 ka) on the Tibetan Plateau, and the main peak covers the period that extends from 12 to 18 ka. Figure 4c shows that young landforms are frequently better preserved than landscapes as a whole, and sampling is easier and more commonly performed on young landforms.

4.2 The results of using different versions of the calculator to estimate ^{10}Be exposure ages

4.2.1 The overall differences in the ^{10}Be exposure ages among different versions of the calculator

Table 2 Statistical results of TCN ^{10}Be exposure ages in Tibetan Plateau

Age range (ka)	<14	14–29	29–57	57–71	71–130	130–191	191–243
MIS Stage	MIS1	MIS2	MIS3	MIS4	MIS5	MIS6	MIS7
Quantity (PCS)	637	531	296	75	176	73	24
Proportion (%)	34.5	28.7	16.0	4.1	9.5	4.0	1.3

Age range (ka)	243–300	300–337	337–374	374–424	424–478	478–533	563–621
MIS Stage	MIS8	MIS9	MIS10	MIS11	MIS12	MIS13	MIS15
Quantity (PCS)	16	5	5	2	5	2	1
Proportion(%)	0.9	0.3	0.3	0.1	0.3	0.1	0.1

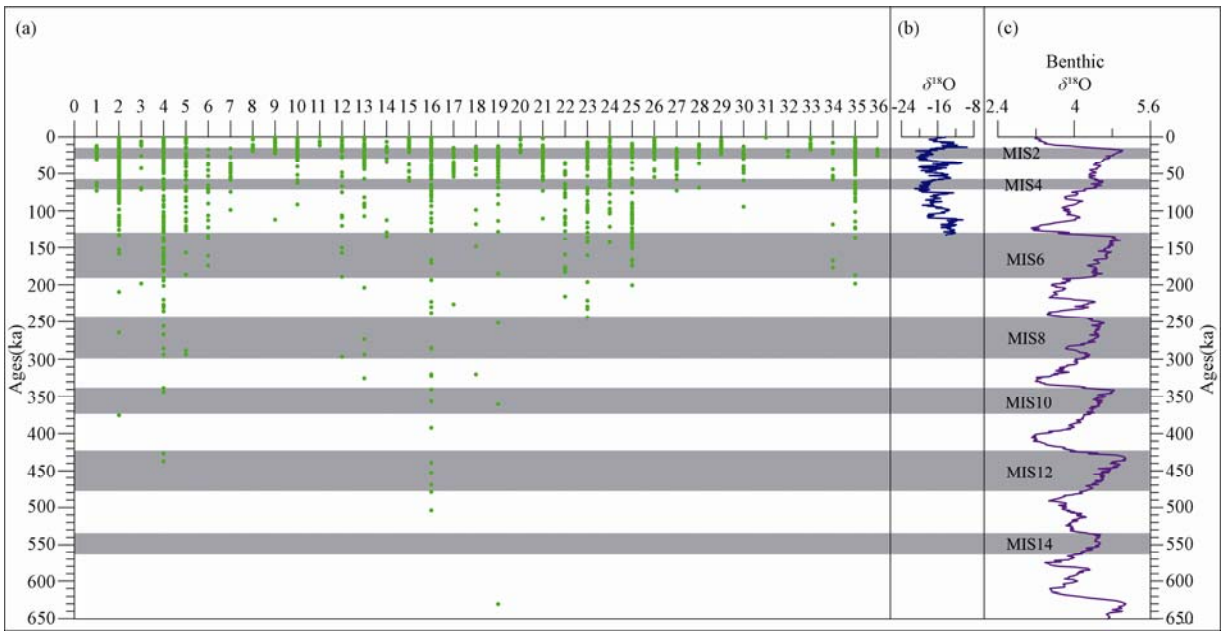

Fig. 3. Comparison of TCN ^{10}Be exposure ages among different regions on the Tibetan Plateau.
(a), Distribution of TCN ^{10}Be exposure ages; (b), δ^{18}O record from the Guliya ice core (Thompson et al., 1997); (c), The stacked Benthic δ^{18}O curve for the past 650 ka (Lisiecki and Raymo, 2005).

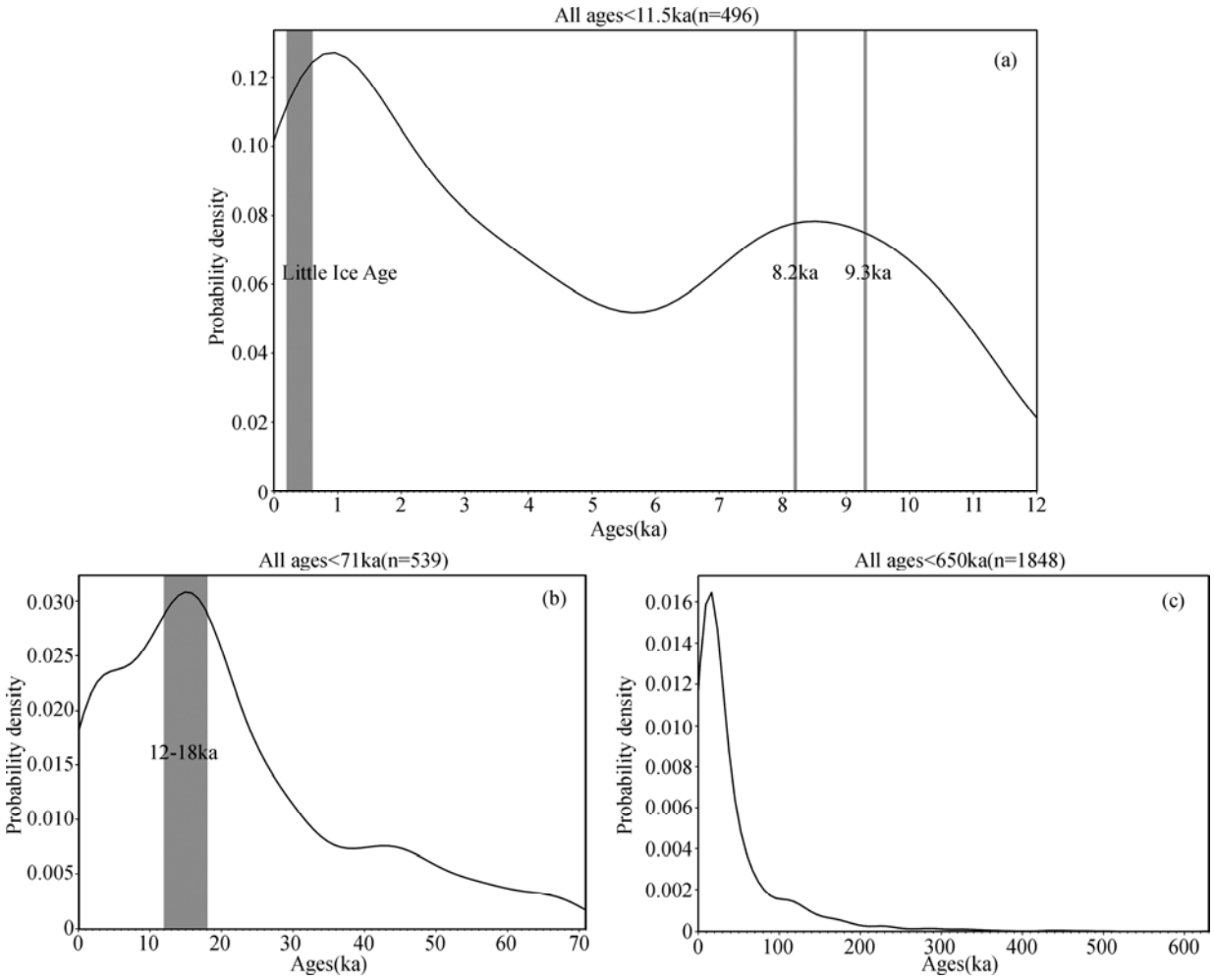

Fig. 4. Probability density curve of TCN ^{10}Be exposure ages in the Tibetan Plateau.
(a), Probability density curve of TCN ^{10}Be exposure ages since 11.5ka; (b), Probability density curve of TCN ^{10}Be exposure ages since 71ka; (c), Probability density curve of TCN ^{10}Be exposure ages since 650ka.

In this paper, 1594 TCN exposure ages obtained from study areas 1–30 were selected to calculate the ^{10}Be exposure ages using the three different versions of the calculator. Due to the differences between regions, the data cannot be compared directly. Therefore, 9 of the study areas were selected at random, and box plots were made for each study area (shown in Fig. 5). The box plots show the maximum, minimum, and median of the ^{10}Be exposure ages within each study area, as well as the upper and lower quartiles. According to the overall observations reported in the 9 randomly selected studies in most regions, the newer versions of the CRONUS-Earth online calculator yield older ^{10}Be exposure ages for individual samples.

4.2.2 Degree of dispersion of the ^{10}Be exposure ages obtained using different versions of the calculator

Keeping the sampling conditions and measured parameters for each sample unchanged, the ^{10}Be exposure ages obtained using the three different versions of the calculator are analyzed using the coefficient of variation; the results are shown in Figure 6a. The coefficients of variation of 1348 of the ages (approximately 84.6% of the total) are less than 0.1, reflecting weak variation; the coefficients of variation of 246 of the ages (approximately 15.4% of the total) are between 0.1 and 1, reflecting moderate variation; none of the coefficients of variation exceed 1. These results indicate that the three different versions represent a steady state in which the degree of dispersion among the ^{10}Be exposure ages obtained for individual samples are relatively small.

4.2.3 The maximum difference among the ^{10}Be ages obtained using different versions of the calculator

Recalculating the ^{10}Be exposure ages of 1594 samples using versions 2.2, 2.3, and 3.0 of the calculator produces three different ^{10}Be exposure ages for each sample. The differences between the three ages are then calculated, and the maximum differences among the ^{10}Be exposure ages from individual samples are obtained (as shown in Fig.

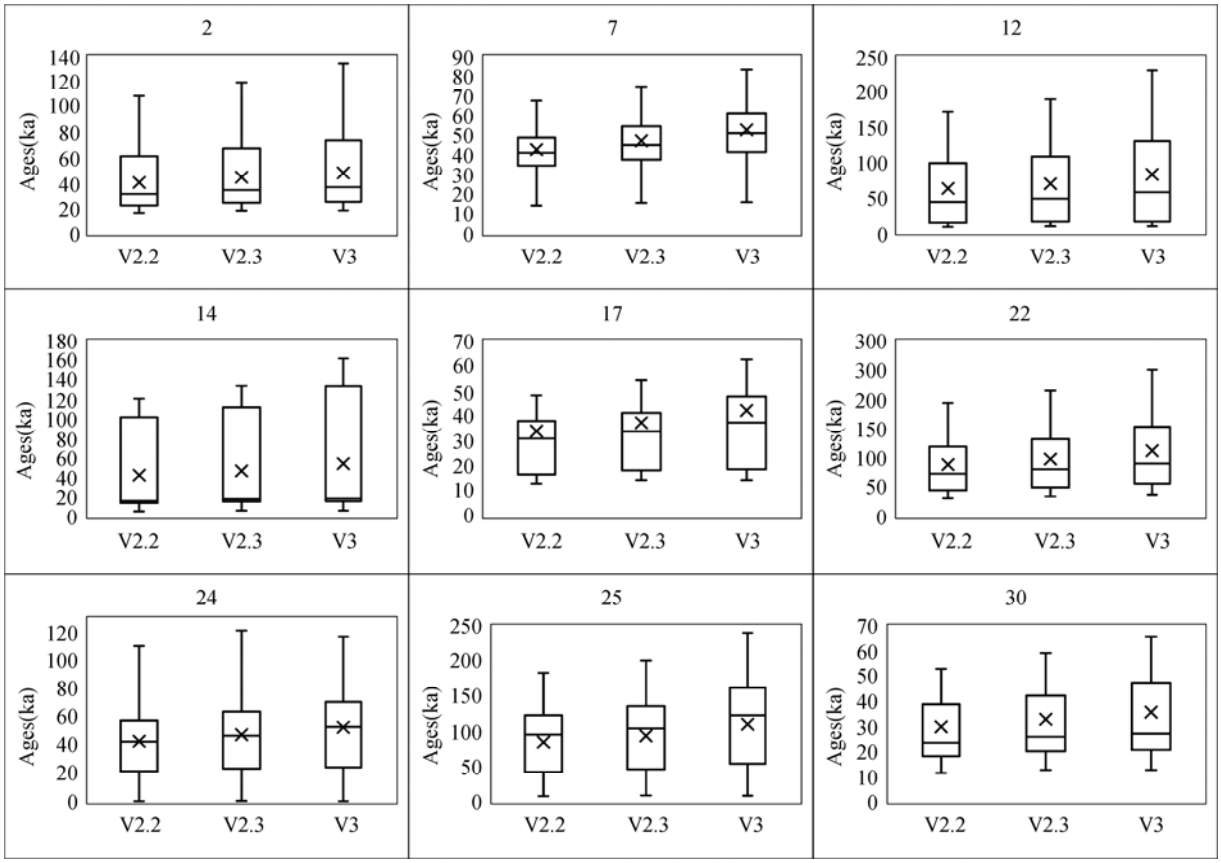

Fig. 5. Box-plot of TCN ^{10}Be exposure age from randomly selected nine study areas (after Mériaux et al., 2004; Owen et al., 2005; Abramowski et al., 2006; Schaefer et al., 2008; Zhou et al., 2007, 2010; Chevalier et al., 2011; Heyman et al., 2011b; Fu et al., 2013; Wang et al., 2013).

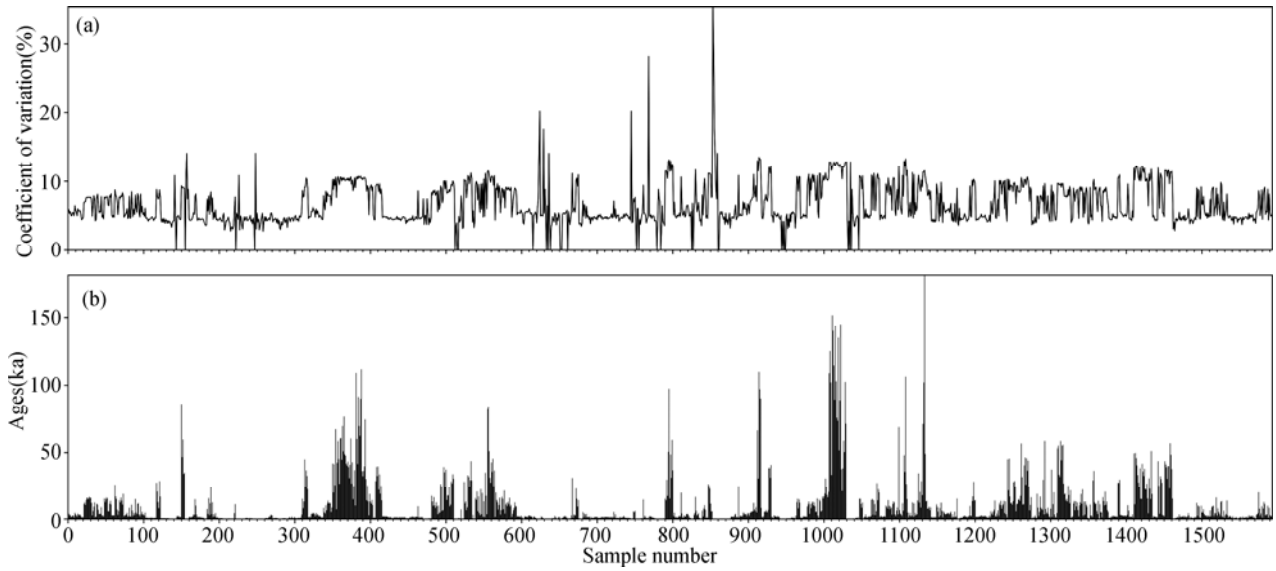

Fig. 6. TCN ^{10}Be exposure ages of different samples.
(a), Coefficient of variation of corresponding different samples; (b), Maximum exposure age of corresponding different samples.

6b). The results show that the maximum differences for 990 of the samples (approximately 62% of the total) are less than 5 ka; the largest differences for 146 of the samples (approximately 9% of the total) range from 5 to 10 ka; and the largest differences for 458 of the samples (approximately 29% of the total) exceed 10 ka. The maximum difference observed for a single sample is 181.1 ka.

5 Discussion

5.1 Analysis of the results of ^{10}Be dating on the Tibetan Plateau

5.1.1 The Last Glacial Maximum on the Tibetan Plateau

Many glacial advances occurred on the Tibetan Plateau during the last glacial period (Finkel et al., 2003; Chevalier et al., 2011; Owen and Dortch, 2014). The Last Glacial Maximum refers to the period during which the coldest climatic conditions and the most extensive glaciation occurred in the last glacial period, similar to Marine Isotope Stage (MIS) 2. Based on the record obtained from the Guliya ice core, this period occurred at 16–32 ka BP on the Tibetan Plateau (Shi Yafeng et al., 1997). The main peak period (12–18 ka) shown in Figure 4b corresponds to a glacial event during the LGM, indicating that glacial deposits produced during the LGM are relatively intact on the Tibetan Plateau, given the accumulation of chronological data at that time. The age of the Dali Ice Age, which represents the last glacial period, has been estimated to be 16 ka by ESR dating (Kuang Mingsheng and Zhao Weicheng, 1997) and 15.7±1.2–18.1±1.36 ka by TL dating (Yang et al., 2006). Wang Jie et al. (2007) measured the exposure ages of outcrops with apparent glacial striations approximately 2 km beyond the termini of modern glaciers in the Tanggula Mountains using the cosmogenic nuclide ^{10}Be; the age of a terminal moraine 5600 m downvalley from the terminus of the Longxiazailongba glacier was also determined using ^{14}C dating. In this study, ages of 16.1±0.3 ka BP and 16.1±0.3 ka BP were obtained, respectively, which correspond to MIS 2. Wang et al. (2006) studied TCN exposure ages obtained from the Shaluli Mountains, which lie on the southeastern margin of the Tibetan Plateau, using cosmogenic ^{10}Be. The results show that the exposure age of the roche moutonnee of Tuershan is 15 ka, which corresponds to the LGM. In addition, the glacial topography of the LGM is preserved in the major mountain ranges of the Tibetan Plateau (Shi Yafeng et al., 2006, 2011). Although the main peak of the exposure ages (12–18 ka) corresponds to the peak of the LGM (16–32 ka BP), some discrepancies remain. The main peak does not correspond to the global LGM (which was centered on 21 ka). Many reasons may have produced this result. First, the samples may have been collected from boulders that became exposed at the surface after the LGM, causing the data to represent underestimates. These samples may also reflect the time when the glaciers began to retreat after reaching their maximum, rather than the LGM. Second, as erosion rates are difficult to estimate, the results of ^{10}Be exposure dating, which typically does not consider erosion, all represent minimum exposure ages; thus, underestimation of the exposure ages may occur, and this effect is more severe on older glacial landforms (Zhang Zhigang et al., 2014a). Furthermore, the development of glaciers is affected by the regional climate, and a local LGM likely occurred (Zhao Jingdong et al., 2011; Dortch et al., 2013; Owen and Dortch, 2014). Li Shijie and Shi Yafeng (1994) argue that regional differences exist in the time when glaciers advanced and reached their maxima during the LGM on the Tibetan Plateau. Shi Yafeng et al. (1997) showed that the glaciers were only 1.9–3.4 times larger than the modern glaciers during the LGM in the extremely dry and cold West Kunlun Mountains and the Qiangtang region in the western Tibetan Plateau. However, in the eastern part of the plateau and the eastern Kunlun Mountains, where the monsoon rainfall is high, the glaciers were 40 to 145 times larger than the modern glaciers during the LGM. Heyman et al. (2011b) combined glacial geology (remote sensing and field studies) and high-resolution glacier simulation experiments to determine the ^{10}Be exposure ages of 67 samples in the Bayan Har Shan in the northeastern Tibetan Plateau. The results show that, during the global LGM, small or no glacier advances occurred in the Bayan Har Shan, which confirms the existence of regional differences in glacier advances on the Tibetan Plateau during the LGM.

5.1.2 Fluctuations of the Holocene glaciers on the Tibetan Plateau

The Holocene is the most recent interglacial period that has occurred during the Quaternary glacial-interglacial cycles; its climate is extremely unstable, and the Holocene is an era of rapid climate change (Mayewski et al., 2004). Many scholars have used ice cores (Yao Tandong and Thompson, 1992; Yao Tandong et al., 1997; Shi Yafeng et al., 1999b), ^{14}C dating (Li Shijie and Jiao Keqin, 1990; Yi et al., 2010), TCN dating (Owen et al., 2008; Owen, 2009b; Seong et al., 2009; Dortch et al., 2013) and other dating methods to identify rapid changes in Holocene climate on the Tibetan Plateau. This paper shows that more peaks occur in the Holocene, indicating that the glaciers on the Tibetan Plateau are sensitive to climate oscillations. The glacial advances of the Holocene can be divided into the Little Ice Age, Neoglacial and early and middle periods (Cui et al., 2011). The Little Ice Age refers to the period of cold climates that extended from the 15th to the 19th century, and modern glaciers in western China generally show 3 to 4 terminal moraines (Su Zhen and Shi Yafeng, 2000; Liu Shiyin et al., 2002). The age at which the first peak in Figure 4a appears is similar to that in the Little Ice Age, suggesting that glacial landforms deposited during the Little Ice Age are preserved on the Tibetan

Plateau. Of these, three moraines preserved around the margins of the Urumqi River Glacier No. 1 on the northern slope of the Karawu Mountains in the northern part of the Tianshan Mountains are well preserved, and their lichen ages are 1538±20 a, 1777±20 a and 1871±20 a, respectively (Chen, 1989). The second peak shown in Figure 4a corresponds to the 8.2 ka and 9.3 ka events, indicating that the glacier advance in the Early Holocene was related to these cooling events. Decreases in temperature may be the main driving force for Holocene glaciations, and it seems reasonable to conclude that the glacier advances in the Holocene were driven by changes in temperature. Seong et al. (2009) used TCN dating to measure the ages of the millennial-scale glacier fluctuations since the LGM in the Kongur Shan and Muztag Ata in the extreme continental glacier region and compared the age results with climatic curves. The results show that, since the LGM, the glaciers in the western Tibetan Plateau have mainly responded to climate fluctuations (rapid cooling events) in the Northern Hemisphere but have been less affected by the South Asian monsoon. Thompson et al. (1997) and Yao Tandong et al. (1997) applied studies of ice cores obtained from the Tibetan Plateau to support the hypothesis that climate changes in this area are associated with mid-latitude westerlies and Atlantic climate changes, and multiple rapid (millennial-centennial) climate fluctuations have occurred. Even in the extreme continental glacier region (where the glaciers are relatively sensitive to precipitation), glacial advances are also mainly driven by changes in temperature. Sati et al. (2014) used OSL dating techniques to conduct chronological studies of the Dinagli Valley in the western Himalayas. The results show that, since 12 ka, the region has experienced three major glaciations at 1 ka, 7.5–4.5 ka and 12–9 ka. In addition, the area also exhibits evidence of glacier advances corresponding to the Little Ice Age, and it is also believed that the combined effects of temperature and precipitation lead to glacial fluctuations in the area, but decreases in temperature are the main driving factor. In summary, combining existing research results and the peaks in the probability density curve generated from the recalculated 1848 ^{10}Be ages on the Tibetan Plateau that correspond to the 8.2 ka and 9.3 ka cold events suggests that reductions in temperature may have been the main driving force of glaciation during the Holocene. Finally, it is particularly noted that the use of probability density curves to extract the true timings of ice ages requires further testing, and Figure 4 does not account for the characteristics of the different regions on the Tibetan Plateau, specifically the heterogeneities caused by local climate conditions and topography. Despite these caveats, the large amounts of data examined in this study have some significance in revealing the overall trends.

5.2 Analysis of the reasons for the differences in the ^{10}Be exposure ages produced by different versions of the calculator

Although the ^{10}Be exposure ages produced by the three different versions of the calculator are relatively tightly clustered, the application of these different versions to individual samples produces large differences in the ^{10}Be exposure ages. Four hundred and fifty-eight of the 1594 samples (approximately 29% of the total) show maximum differences greater than 10 ka, and the maximum difference observed for a single sample is 181.1 ka, which has a significant impact on determining the exposure ages of glacial deposits. The reasons for the discrepancy stem from the constant updates to the CRONUS-Earth online calculator; version 2.2 included incorrect default calibration data and inaccurate scaling schemes, as well as erroneous muon interaction cross sections (Marrero et al., 2016). Version 2.3 is more accurate than the previous versions of the CRONUS-Earth calculator. It updates the cross-section data for muon interactions with data obtained from Borchers et al. (2016), who performed a calibration using data from the Beacon Heights bedrock core. The use of these data may have a significant impact on areas with relatively high erosion rates (Heisinger et al., 2002). Version 2.3 of the calculator also uses the new ^{10}Be and ^{26}Al default reference production rates, corrects the Be and Al measurement standards used in version 2.2, and addresses other errors (Marrero et al., 2016), all of which provide additional corrections to the TCN ages. Version 3.0 is maintains acceptable accuracy while rapidly calculating exposure ages. Because the version 3.0 release only became available in March 2017, its accuracy and reliability have not been extensively tested (Balco, 2017). In addition to the different versions discussed in this article, which produce ^{10}Be ages that differ by as much as 181.1 ka, Owen et al.(2008) showed that different production rate models can also result in 30% or even 40% differences in ages. Regardless of the model or production rates used, geomorphological uncertainties and the use of different metrics of landform age have more significant effects on the estimated ages of glacial landforms (Owen and Dortch, 2014). On the one hand, geological and topographic factors are the largest sources of uncertainty in the ^{10}Be exposure dating method (Briner et al., 2005; Owen et al., 2008; Heyman et al., 2011a; Dortch et al., 2013; Murari et al., 2014). Pre-depositional exposure can lead to the overestimation of ages, whereas other factors (the instability of boulders on moraines, erosion, weathering, subsequent exhumation, snow cover or

sediment cover) can lead to the underestimation of such ages. On the other hand, many scholars believe that the methods used to calculate the ages of landforms from exposure ages affect the inferred ages of glacial landforms. Examples include the mean standard weighted deviation (MSWD) method, which simplifies the identification of outlier exposure ages (Finkel et al., 2003; Hedrick et al., 2011). Dortch et al. (2013) combined the Gaussian distribution with the cumulative probability density function to obtain the best fit to TCN exposure ages in the western semiarid region of the Tibetan Plateau and used the result to partition the local ice age. Student's t -test has also been used to analyze TCN chronological data in nearby areas (Owen and Dortch, 2014). In conclusion, in addition to the limitations on the results of TCN dating imposed by basic physical principles and geological uncertainty, researchers choose different methods of statistical analysis and different versions of the online calculator, and other factors can also have an impact. The continuous updates to the CRONUS-Earth online calculator lead to differences among the ^{10}Be exposure ages produced by the three different versions of the calculator, and the factors that were changed during these updates are numerous and complex.

6 Conclusions

This paper recalculates ^{10}Be ages obtained from the Tibetan Plateau published during 1999–2017 using three different versions of the CRONUS-Earth online calculator and combines them with existing research results. The following conclusions can be drawn from this work.

(1) Boulder dating samples make up for 97% of the dataset, and approximately 97% of the exposure ages are less than 200 ka. (2) The probability density curve of the exposure ages suggests that greater numbers of oscillations emerge during the Holocene, and the peaks correspond to the Little Ice Age and the 8.2 ka and 9.3 ka cold events. We infer that several glacier advances occurred on the Tibetan Plateau during the Holocene, and the occurrence of these multiple events is closely related to the rapid climate change events in the Holocene. Cooling is probably the main driving factor of Holocene glaciation. In addition, the main peak corresponds to 12–18 ka, which may correspond to the height of the Last Glacial Maximum, but there is a discrepancy, and no major peak can be identified that corresponds to the global Last Glacial Maximum, which was centered on 21 ka. (3) For most regions, the newer versions of the CRONUS-Earth calculator produce older ^{10}Be ages for the same samples. Given the different versions of the CRONUS-Earth online calculator, the maximum differences for approximately 29% of the ^{10}Be ages exceed 10 ka, and the largest difference for an individual sample is 181.1 ka.

Although the TCN dating technique is one of the most successful dating techniques used in the study of Quaternary glacial history, the accuracy of these determinations is restricted by many factors. Therefore, improving the accuracy of the TCN dating technique for application to Quaternary glacial landforms and establishing more accurate geochronological frameworks still requires further work by additional researchers.

Acknowledgements

This work was supported by the National Natural Science Foundation of China (Grant No. 41503054), the China Postdoctoral Science Foundation (2015M582728), the Priority Academic Program Development of Jiangsu Higher Education Institutions (PAPD) (Grant No. 164320H116), and by the Yulong Mountain tourism development and management committee special project.

Manuscript received Feb. 24, 2018
accepted Mar. 10, 2018
edited by Fei Hongcai

References

Abramowski, U., 2004. *The use of ^{10}Be surface exposure dating of erratic boulders in the reconstruction of the late Pleistocene glaciation history of mountainous regions, with examples from Nepal and Central Asia*. University of Bayreuth (Ph.D Thesis).

Abramowski, U., Bergau, A., Seebach, D., Zech, R., Glaser, B., Sosin, P., Kubik, P.W., and Zech, W., 2006. Pleistocene glaciations of Central Asia: results from ^{10}Be surface exposure ages of erratic boulders from the Pamir (Tajikistan) and the Alay-Turkestan range (Kyrgyzstan). *Quaternary Science Reviews*, 25(9/10): 1080–1096.

Aoki, T., and Imamura, M., 1999. Reconstructing the glacial chronology based on the ^{10}Be exposure age—the case study of the Khumbu Glacier, eastern Nepal Himalayas. *Bulletin of the National Museum of Japanese History*, 81: 517–525.

Balco, G., 2017. Production rate calculations for cosmic-ray-muon-produced ^{10}Be and ^{26}Al benchmarked against geological calibration data. *Quaternary Geochronology*, 39.

Balco, G., Stone, J.O., Lifton, N.A., and Dunai, T.J., 2008. A complete and easily accessible means of calculating surface exposure ages or erosion rates from Be-10 and Al-26 measurements. *Quaternary Geochronology*, 3(3): 174–195.

Barnard, P.L., Owen, L.A., Sharma, M.C., and Finkel, R.C., 2004. Late Quaternary landscape evolution of a monsoon-influenced high Himalayan valley, Gori Ganga, Nanda Devi, NE Garhwal. *Geomorphology*, 61(1/2): 91–110.

Barnard, P.L., Owen, L.A., Finkel, R.C., and Asahi, K., 2006. Landscape response to deglaciation; in a high relief, monsoon-influenced alpine environment, Langtang Himal, Nepal. *Quaternary Science Reviews*, 25(17/18): 2162–2176.

Borchers, B., Marrero, S., Balco, G., Caffee, M., Goehring, B., Lifton, N., Nishiizumi, K., Phillips, F., Schaefer, J., and Stone, J., 2016. Geological calibration of spallation production rates in the cronus-earth project. *Quaternary Geochronology*, 31(4): 188–198.

Briner, J.P., Kaufman, D.S., Manley, W.F., Finkel, R.C., and Caffee, M.W., 2005. Cosmogenic exposure dating of late Pleistocene moraine stabilization in Alaska. *Geological Society of America Bulletin*, 117(7): 1108–1120.

Brown, E.T., Bendick, R., Bourles, D.L., Gaur, V., Molnar, P., Raisbeck, G.M., and Yiou, F., 2002. Slip rates of the Karakorum fault, Ladakh, India, determined using cosmic ray exposure dating of debris flows and moraines. *Journal of Geophyscial Research*, 107(B9):1–9.

Chen Guohui and Ma Ling, 2017. The follower of the "dream of ice core"-Yao Tandong, the director of the Institute of the Tibetan Plateau Research Institute of the Chinese Academy of Sciences and the academician of the Chinese Academy of Sciences. *Technology and Industry Across The Strait*, (2): 4–6 (in Chinese with English abstract).

Chen Jiyang, 1989. Preliminary researches on lichenometric chronology of Holocene glacial fluctuations and on other topics in the headwater of Urumqi River, Tianshan Mountains. *Science in China: Series B*, 32(12): 1487–1500.

Chevalier, M.L., Hilley, G., Tapponnier, P., Woerd, J.V.D., Zeng Jingliu, Finkel, R.C., Ryerson, F.J., Li Haibing and Liu Xiaohan, 2011. Constraints on the late Quaternary glaciations in Tibet from cosmogenic exposure ages of moraine surfaces. *Quaternary Science Reviews*, 30(5/6): 528–554.

Colgan, P.M., Munroe, J.S., and Zhou Shangzhe, 2006. Cosmogenic radionuclide evidence for the limited extent of last glacial maximum glaciers in the Tanggula Shan of the central Tibetan Plateau. *Quaternary Researc*h, 65(2), 336–339.

Cressie, N., 1992. Statistics for spatial data. Technometrics, 35 (3): 321–323.

Cui Zhijiu, Chen Yixin, Zhang Wei, Zhou Shangzhe, Zhou Liping, Zhang Mei and Li Chuanchuan, 2011. Research history, glacial chronology and origins of Quaternary glaciations in China. *Quaternary Science*s, 31(5): 749–764.

Dong Guocheng, Yi Chaolu and Caffee, M.W., 2014. ^{10}Be dating of boulders on moraines from the last glacial period in the Nyainqentanglha mountains, Tibet. *Science China Earth Sciences*, 57(2): 221–231.

Dong Guocheng, Zhou Weijian, Yi Chaolu, Zhang Li, Li Ming, Fu Yunchong and Zhang Qian, 2017a. Cosmogenic ^{10}Be surface exposure dating of 'Little Ice Age' glacial events in the Mount Jaggang area, central Tibet. *Holocene*, 27(10), 095968361769389.

Dong Guocheng, Xu Xiangke, Zhou Weijian, Fu Yunchong, Zhang Li and Li Ming, 2017b. Cosmogenic ^{10}Be surface exposure dating and glacier reconstruction for the Last Glacial Maximum in the Quemuqu Valley, western Nyainqentanglha Mountains, south Tibet. *Journal of Quaternary Science*, 32(5).

Dortch, J.M., Owen, L.A., and Caffee, M.W., 2010. Quaternary glaciation in the Nubra and Shyok valley confluence, northernmost Ladakh, India. *Quaternary Research*, 74(1): 132–144.

Dortch, J.M., Owen, L.A., and Caffee, M.W., 2013. Timing and climatic drivers for glaciation across semiarid western Himalayane Tibetan orogen. *Quaternary Science Reviews*, 78 (11): 188–208.

Dyke, A.S., Andrews, J.T., and Clark, J.H., 2002. The Lauentide and Innuitian ice sheets during the last Glacial Maximum. *Quaternary Science Reviews*, (21): 9–31.

Dyurgerov, M.B., and Meier, M.F., 2005. *Glaciers and the Changing Earth System: A 2004 Snapshot*. Institute of Arctic and Alpine Research, University of Colorado, USA.

Finkel, R.C., Owen, L.A., Barnard, P.L., and Caffee, M.W., 2003. Beryllium-10 dating of Mount Everest moraines indicates a strong monsoonal influence and glacial synchroneity throughout the Himalaya. *Geology*, 31(6): 561–564.

Fu Ping, Stroeven, A.P., Harbor, J.M., Hättestrand, C., Heyman, J., Caffee, M.W., and Zhou Liping, 2013. Paleoglaciation of Shaluli Shan, Southeastern Tibetan Plateau. *Quaternary Science Reviews*, 64: 121–135.

Gayer, E., Lavé, J., Pik, R., and France-Lanord, C., 2006. Monsoonal forcing of Holocene glacier fluctuations in Ganesh Himal (central Nepal) constrained by cosmogenic ^{3}He exposure ages of garnets. *Earth & Planetary Science Letters*, 252(3/4): 275–288.

Gosse, J.C., and Phillips, F.M., 2001. Terrestrial in situ cosmogenic nuclides: theory and application. *Quaternary Science Reviews,* 20(14): 1475–1560.

Graf, A. A., Strasky, S., Zhao Zhizhong, Akcar, N., Ivy-Ochs, S., Kubik, P.W., Christl, M., Kasper, H.U., Wieler, R., and Schlüchter, C., 2008. Glacier extension on the eastern Tibetan Plateau in response to MIS 2 cooling, with a contribution to ^{10}Be and ^{21}Ne methodology. In: Strasky, S. (ed.), *Glacial response to global climate changes: cosmogenic nuclide chronologies from high and low latitudes*. ETH Zürich (PhD Thesis).

Grin, E., Ehlers, T.A., Schaller, M., Sulaymonova, V., Ratschbacher, L., and Gloaguen, R., 2016. ^{10}Be Surface-Exposure Age Dating of the Last Glacial Maximum in the Northern Pamir (Tajikistan). *Quaternary Geochronology*, 34: 47–57.

Hedrick, K.A., Seong, Y.B., Owen, L.A., Caffee, M.W., and Dietsch, C., 2011. Towards defining the transition in style and timing of Quaternary glaciation between the monsoon-influenced Greater Himalaya and the semi-arid Transhimalaya of Northern India. *Quaternary International*, 236(1/2): 21–33.

Heisinger, B., Lal, D., Jull, A.J.T., Kubik, P., Ivy-Ochs, S., Knie, K., and Nolte, E., 2002. Production of selected cosmogenic radionuclides by muons: 2. capture of negative muons. *Earth & Planetary Science Letters*, 200(3): 357–369.

Heyman, J., Stroeven, A., Harbor, J., and Caffee, M.W., 2011a. Too young or too old: evaluating cosmogenic exposure dating based on an analysis of compiled boulder exposure ages. *Earth and Planetary Science Letters*, 302(1/2): 71–80.

Heyman, J., Stroeven, A.P., Caffee, M.W., Hättestrand, C., Harbor, J.M., Li Yingkui, Alexanderson, H., Zhou Liping and Hubbard, A., 2011b. Palaeoglaciology of Bayan Har Shan, NE Tibetan Plateau: exposure ages reveal a missing LGM expansion. *Quaternary Science Reviews*, 30(15/16): 1988–2011.

Heyman, J., 2014. Paleoglaciation of the Tibetan Plateau and surrounding mountains based on exposure ages and ela depression estimates. *Quaternary Science Reviews*, 91(3): 30–41.

Hu Gang, Yi Chaolu, Zhang Jiafu, Dong Guocheng, Liu Jinhua,

Xu Xiangke and Jiang Tao, 2016. Extensive glacial advances during the Last Glacial Maximum near the eastern Himalayan syntaxis. *Quaternary International*.

Kind, R., Yuan, X., Saul, J., Nelson, D., Sobolev, S.V., Mechie, J., Zhao, W., Kosarev, G., Ni, J., Achauer, U., and Jiang, M., 2002. Seismic images of crust and upper mantle beneath Tibet: evidence for eurasian plate subduction. *Science*, 298 (5596): 1219.

Kong Ping, David, F., Na Chunguang and Huang Feixin, 2009a. Late quaternary glaciation of the tianshan, central asia, using cosmogenic ^{10}Be surface exposure dating. *Quaternary Research*, 72(2): 229–233.

Kong Ping, Na Chunguang, Fink, D., Zhao Xitao and Xiao Wei, 2009b. Moraine dam related to late Quaternary glaciation in the Yulong Mountains, southwest China, and impacts on the Jinsha River. *Quaternary Science Reviews*, 28(27/28): 3224–3235.

Kuang Mingsheng and Zhao Weicheng, 1997. Study on ESR dating of depositional stratums of late Pleistocene epoch in Diancangshan area about Dali city in Yunnan Province. *Yunnan Geographic Environment Research*, 9(1): 49–57 (in Chinese with English abstract).

Lal, D., 1991. Cosmic ray labeling of erosion surfaces: in situ nuclide production rates and erosion models. *Earth & Planetary Science Letters*, 104(91): 424–439.

Lasserre, C., Gaudemer, Y., Tapponnier, P., Mériaux, A.S., Van der Woerd, J., Yuan Daoyang, Ryerson, F.J., Finkel, R.C., and Caffee, M.W., 2002. Fast late Pleistocene slip rate on the Leng Long Ling segment of the Haiyuan fault, Qinghai, China. *Journal of Geophysical Research*, 107(B11): 2276–2291.

Li Jian, Zhang Yueqiao, Li Hailong, Xiong Jinhong, Li Jianhua and Wu Tairan, 2016a. Revisiting late quaternary slip-rate along the Maqu Segment of the Eastern Kunlun Fault, Northeast Tibet. *Acta Geologica Sinica* (English Edition), 90 (2): 486–502.

Li Shijie and Jiao Keqin, 1990. Glacier variations on the south slope of West Kunlun Mountains since 30000 years. *Journal of Glaciology and Geocryology*, 12(4): 311–318 (in Chinese with English abstract).

Li Shijie and Shi Yafeng, 1994. *Regional differentiation of the glacial development and climatic environment in the last glacial maximun on the Tibet Plateau*. Beijing: China Academic Journal Electronic Publishing House (in Chinese with English abstract).

Li Yanan, Li Yingkuai, Harbor, J., Liu Gengnian, Yi Chaolu and Caffee, M.W., 2016b. Cosmogenic ^{10}Be constraints on Little Ice Age glacial advances in the eastern Tian Shan, China. *Quaternary Science Reviews*, 138: 105–118.

Li Yingkuai, Liu Gengnian, Kong Ping, Harbor, J., Chen Yixin and Caffee, M.W., 2011. Cosmogenic nuclide constraints on glacial chronology in the source area of the Urumqi River, Tian Shan, China. *Journal of Quaternary Science*, 26(3): 297–304.

Li Yingkuai, Liu Gengnian, Chen Yixin, Li Yanan, Harbor, J., Stroeven, A.P., Caffee, M.W., Zhang Mei, Li Chuanchuan and Cui Zhijiu, 2014. Timing and extent of Quaternary glaciations in the Tianger Range, eastern Tian Shan, China, investigated using ^{10}Be surface exposure dating. *Quaternary Science Reviews*, 98: 7–23.

Lifton, N., Beel, C., Hättestrand, C., Kassab, C., Rogozhina, I., Heermance, R., Oskin, M., Burbank, D., Blomdin, R., Gribenski, N., Caffee, M., Goehring, B.M., Heyman, J., Ivanov, M., Li Yanan, Li Yingkui, Petrakov, D., Usubaliev, R., Codilean, A.T., Chen Yixin, Harbor, J., and Stroeven, A.P., 2014. Constraints on the late Quaternary glacial history of the Inylchek and Sary-Dzaz valleys from in situ, cosmogenic ^{10}Be and ^{26}Al, eastern Kyrgyz Tian Shan. *Quaternary Science Reviews*, 101(101): 77–90.

Lisiecki, L.E., and Raymo, M.E., 2005. A Pliocene–Pleistocene stack of 57 globally distributed benthic δ^{18}O records. *Paleoceanography*, 20(PA1003): 1–17.

Liu Shiyin, Shen Yongping, Sun Wenxin and Li Gang. 2002. Glacier Variation since the Maximum of the Little Ice Age in the Western Qilian Mountains, Northwest China. *Journal of Glaciology and Geocryology*, 24(3): 227–233 (in Chinese with English abstract).

Marrero, S.M., Phillips, F.M., Borchers, B., Lifton, N., Aumer, R., and Balco, G., 2016. Cosmogenic nuclide systematics and the cronuscalc program. *Quaternary Geochronology*, 31: 160–187.

Mayewski, P.A., Rohling, E.E., Stager, C.J., Karlén, W., Maasch, A., Meeker, L.D., Meyerson, E.A., Gasse, F., Van Kreveld, S., Holmgren, K., Lee-Thorp, J., Rosqvist, G., Rack, F., Staubwasser, M., Schneider, R.R., and Steig, E.J., 2004. Holocene climate variability. *Quaternary Research*, 62(3): 243–255.

Mériaux, A.S., Ryerson, F.J., Tapponnier, P., Van der Woerd, J., Finkel, R.C., Xu Xiwei, Xu Zhiqin and Caffee, M.W., 2004. Rapid slip along the central Altyn Tagh Fault: morphochronologic evidence from Cherchen He and Sulamu Tagh. *Journal of Geophysical Research*, 109 (B06)401: 1–23.

Murari, M.K., Owen, L.A., Dortch, J.M., Caffee, M.W., Dietsch, C., Fuchs, M., Haneberg, W.C., Sharma, M.C., and Townsend -Small, A., 2014. Timing and climatic drivers for glaciation across monsoon-influenced regions of the Himalayane Tibetan orogen. *Quaternary Science Reviews*, 88(6): 159–182.

Owen, L.A., Robinson, R., Benn, D.I., Finkel, R.C., Davis, N.K., Yi Chaolu, Putkonen, J., Li Dewen and Murray, A.S., 2009a. Quaternary glaciation of Mount Everest. *Quaternary Science Reviews*, 28(15/16): 1412–1433.

Owen, L.A., 2009b. Latest Pleistocene and Holocene glacier fluctuations in the Himalaya and Tibet. *Quaternary Science Reviews*, 28(21): 2150–2164.

Owen, L.A., and Dortch, J.M., 2014. Nature and timing of Quaternary glaciation in the Himalayan-Tibetan orogen. *Quaternary Science Reviews*, 88(88): 14–54.

Owen, L.A., Caffee, M.W., Finkel, R.C., and Seong, B.Y., 2008. Quaternary glaciations of the Himalayane Tibetan orogen. *Journal of Quaternary Science*, 23: 513–532.

Owen, L.A., Finkel, R.C., Caffee, M.W., and Gualtieri, L., 2002. Timing of multiple Late Quaternary glaciations in the Hunza Valley, Karakoram Mountains, northern Pakistan: defined by cosmogenic radionuclide dating of moraines. *Geological Society of America Bulletin*, 114(5): 593–604.

Owen, L.A., Yi Chaolu, Finkel, R.C., and Davis, N.K., 2010. Quaternary glaciation of Gurla Mandhata (Naimon'anyi). *Quaternary Science Reviews*, 29(15/16): 1817–1830.

Owen, L.A., Gualtieri, L., Finkel, R.C., Caffee, M.W., Benn, D.I., and Sharma, M.C., 2001. Cosmogenic radionuclide dating of glacial landforms in the Lahul Himalaya, northern India: defining the timing of late Quaternary glaciations.

Journal of Quaternary Science, 16(6): 555–563.

Owen, L.A., Finkel, R.C., Barnard, P.L., Ma Haizhou, Asahi, K., Caffee, M.W., and Derbyshire, E., 2005. Climatic and topographic controls on the style and timing of Late Quaternary glaciation throughout Tibet and the Himalaya defined by ^{10}Be cosmogenic radionuclide surface exposure dating. *Quaternary Science Reviews*, 24(12/13): 1391–1411.

Owen, L.A., Finkel, R.C., Ma Haizhou, Spencer, J.Q., Derbyshire, E., Barnard, P., and Caffee, M.W., 2003a. Timing and style of Late Quaternary glaciation in northeastern Tibet. *Geological Society of America Bulleti*n, 115(11): 1356–1364.

Owen, L.A., Ma Haizhou, Derbyshire, E., Spencer, J.Q., Barnard, P.L., Nian Zengyong, Finkel, R.C., and Caffee, M.W., 2003b. The timing and style of Late Quaternary glaciation in the La Ji Mountains, NE Tibet: evidence for restricted glaciation during the latter part of the Last Glacial. *Zeitschrift für Geomorphologie*, 130: 263–276.

Owen, L.A., Spencer, J.Q., Ma Haizhou, Barnard, P., Derbyshire, E., Finkel, R.C., Caffee, M.W., and Nian Zengyong, 2003c. Timing of Late Quaternary glaciation along the southwestern slopes of the Qilian Shan, Tibet. *Boreas*, 32: 281–291.

Owen, L.A., Caffee, M.W., Bovard, K.R., Finkel, R.C., and Sharma, M.C., 2006a. Terrestrial cosmogenic nuclide surface exposure dating of the oldest glacial successions in the Himalayan orogen Ladakh Range, northern India. *Geological Society of America Bulletin*, 118(3/4): 383–392.

Owen, L.A., Finkel, R.C., Ma Haizhou and Barnard, P.L., 2006b. Late Quaternary landscape evolution in the Kunlun Mountains and Qaidam Basin, Northern Tibet: a framework for examining the links between glaciation, lake level changes and alluvial fan formation. *Quaternary International*, 154/155: 73–86.

Owen, L.A., Chen Jie, Hedrick, K.A., Caffee, M.W., Robinson, A.C., Schoenbohm, L.M., Yuan Zhaode, Li Wenqiao, Imrecke, D.B., and Liu Jinfeng, 2012. Quaternary glaciation of the Tashkurgan Valley, Southeast Pamir. *Quaternary Science Reviews*, 47(30): 56–72.

Phillips, W.M., Sloan, V.F., Shroder Jr, J.F., Sharma, P., Clarke, M.L., and Rendell, H.M., 2000. Asynchronous glaciation at Nanga Parbat, northwestern Himalaya Mountains, Pakistan. *Geology*, 28(5): 431–434.

Pratt-Sitaula, B., 2005. Glaciers, climate, and topography in the Nepalese Himalaya. University of California, Santa Barbara, PhD Thesis.

Rades, E.F., Hetzel, R., Strobl, M., Xu Qiang and Ding Lin, 2015. Defining rates of landscape evolution in a south Tibetan graben with in situ-produced cosmogenic ^{10}Be. *Earth Surface Processes & Landforms*, 40(14): 1862–1876.

Sati, S.P., Ali, S.N., Rana, N., Bhattacharya, F., Bhushan, R., Shukla, A.D., Sundriyal, Y., and Juyal, N., 2014. Timing and extent of Holocene glaciations in the monsoon dominated Dunagiri valley (Bangni glacier), Central Himalaya, India. *Journal of Asian Earth Sciences*, 91(3): 125–136.

Schäfer, J.M., 2000. *Reconstruction of landscape evolution and continental paleoglaciations using in situ cosmogenic nuclides: examples from Antarctica and the Tibetan Plateau*. ETH Zürich (PhD Thesis).

Schaefer, J.M., Oberholzer, P., Zhao Zhizhong, Ivy-Ochs, S., Wieler, R., Baur, H., Kubik, P.W., and Schluchter, C., 2008. Cosmogenic beryllium-10 and neon-21 dating of late Pleistocene glaciations in Nyalam, monsoonal Himalayas. *Quaternary Science Reviews*, 27(3/4): 295–311.

Schäfer, J.M., Tschudi, S., Zhao Zhizhong, Wu Xihao, Ivy-Ochs, S., Wieler, R., Baur, H., Kubik, P.W., and Schluchter, C., 2002. The limited influence of glaciations in Tibet on global climate over the past 170000 yr. *Earth and Planetary Science Letters*, 194(3/4): 287–297.

Scherler, D., Bookhagen, B., Strecker, M.R., Von Blanckenburg, F., and Rood, D., 2010. Timing and extent of late Quaternary glaciation in the western Himalaya constrained by ^{10}Be moraine dating in Garhwal, India. *Quaternary Science Reviews*, 29(7/8): 815–831.

Seong, Y.B., Owen, L.A., Yi Chaolu and Finkel, R.C., 2009. Quaternary glaciation of Muztag Ata and Kongur Shan: evidence for glacier response to rapid climate changes throughout the Late Glacial and Holocene in westernmost Tibet. *Geological Society of America Bulletin*, 121(3/4): 348–365.

Seong, Y.B., Owen, L.A., Bishop, M.P., Bush, A., Clendon, P., Copland, L., Finkel, R., Kamp, U., and Shroder Jr, J.F., 2007. Quaternary glacial history of the Central Karakoram. *Quaternary Science Reviews*, 26(25/28): 3384–3405.

Shi Yafeng, Zheng Benxing and Yao Tandong, 1997. Glaciers and Environments during the Last Glacial Maximum (LGM) on the Tibetan Plateau. *Journal of Glaciology and Geocryology*, 19(2): 97–113 (in Chinese with English abstract).

Shi Yafeng, Cui Zhijiu and Su Zhen, 2006. *The Quaternary Glaciations and Environmental Variations in China*. Shijiazhuang: Hebei Science and Technology Publishing House, 1–618.

Shi Yafeng, Zhao Jingdong and Wang Jie, 2011. *New Understanding of Quaternary Glaciations in China*. Shanghai: Shanghai Popular Science Press, 1–213.

Shi Yafeng, Li Jijun, Li Bingyuan, Yao Tandong, Wang Suming, Li Shijie, Cui Zhijiu, Wang Fubao, Pan Baotian, Fang Xiaomin and Zhang Qingsong, 1999a. Uplift of the Tibetan Plateau and east Asia environmental change during late cenozoic. *Acta Geographica Sinica*, 54(1): 10–20 (in Chinese with English abstract).

Shi Yafeng, Yao Tandong and Yang Bao, 1999b. Climate change in 2000a Guliya 10a scale and compared with literature records of Eastern China. *Science in China* (Series D), 29: 79 (in Chinese).

Stone, J.O., 2000. Air pressure and cosmogenic isotope production. *Journal of Geophysical Research*, 105(B10): 23753–23759.

Strasky, S., Graf, A.A., Zhao Zhizhong, Kubik, P.W., Baur, H., Schluchter, C., and Wieler, R., 2009. Late glacial ice advances in southeast Tibet. *Journal of Asian Earth Science*s, 34(3): 458–465.

Stübner, K., Grin, E., Hidy, A.J., Schaller, M., Gold, R.D., Ratschbacher, L., and Ehlers, T., 2017. Middle and Late Pleistocene glaciations in the southwestern Pamir and their effects on topography. *Earth & Planetary Science Letters,* 466: 181–194.

Su Zhen and Shi Yafeng, 2000. Response of monsoonal temperate glaciers in China to global warming since the Little Ice Age. *Journal of Glaciology and Geocryology*, 22(3): 223–229 (in Chinese with English abstract).

Tang Wenqing, Zhang Yongshuang, Zhang Qingzhi, Zhou

Hongfu, Pan Zhongxi, Li Jun and Yang Cheng, 2016. Present-day block movement and fault activity on the eastern margin of the Tibetan Plateau. *Acta Geologica Sinica* (English Edition), 90(2): 456–466.

Thompson, L.G., Yao Tandong, Davis, M.E., Henderson, K.A., Mosley-Thompson, E., Lin, P.N., Beer, J., Synal, H.A., Cole-Dai, J., and Bolzan, J.F., 1997. Tropical climate instability: the Last Glacial Cycle from a Qinghai-Tibetan ice core. *Science*, 276(5320): 1821–1825.

Tschudi, S., Schäfer, J.M., Zhao Zhizhong, Wu Xihao, Ivy-Ochs, S., Kubik, P.W., and Schluchter, C., 2003. Glacial advances in Tibet during the Younger Dryas? Evidence from cosmogenic ^{10}Be, ^{26}Al, and ^{21}Ne. *Journal of Asian Earth Sciences*, 22(4): 301–306.

Wang Jian, Raisbeck, G., Xu Xiaobin, Yiou, F., and Bai Shibiao, 2006. In situ cosmogenic ^{10}Be dating of the Quaternary glaciations in the southern Shaluli Mountain on the southeastern Tibetan Plateau. *Science in China. Series D: Earth Sciences*, 49 (12): 1291–1298.

Wang Jian, Zhang Zhigang, Xu Xiaobin, Kong Ping, Bai Shibiao, Zhang Maoheng and Liang Zhong, 2012. Cosmogenic isotopes dating of Quaternary glacial activity of the Paleao-Daocheng ice cap on the southeastern part of the Qinghai-Xizang Plateau. *Quaternary Sciences*, 32(3): 394–402 (in Chinese with English abstract).

Wang Jie and Zhou Shangzhe, 2009. Cosmogenic Nuclides Method Applied to Quaternary Glaciation Dating: Review and Prospect. *Journal of Glaciology and Geocryology*, 31(3): 501–509 (in Chinese with English abstract).

Wang Jie, Zhou Shangzhe, Tang Shulin, Colgan, P.M., and Munroe, J.S., 2007. The Sequence of Quaternary Glaciations around the Tanggula Pass. *Journal of Glaciology and Geocryology*, 29(1): 149–155 (in Chinese with English abstract) .

Wang Jie, Kassab, C., Harbor, J.M., Caffee, M.W., Cui Hang and Zhang Guoliang, 2013. Cosmogenic nuclide constraints on late Quaternary glacial chronology on the Dalijia Shan, northeastern Tibetan Plateau. *Quaternary Research*, 79(3): 439–451.

Wu Zhonghai, Zhao Xitao, Jiang Wan, Wu Zhenhan and Zhu Dagang, 2003. Dating result of the Pleistocene glacial deposits on the southeast foot of Nyaiqentanglha Mountains. *Journal of Glaciology and Geocryology*, 25(3): 272–274 (in Chinese with English abstract).

Xin Chunlei, 2016. Uncertainty of TCN technology in the dating of Glacial Geomorphology. *Journal of Mudanjiang Teachers College* (Natural Sciences Edition), (2): 33–34 (in Chinese with English abstract).

Xu Xiangke, Hu Gang and Qiao Baojin, 2013. Last glacial maximum climate based on cosmogenic ^{10}Be exposure ages and glacier modeling for the head of Tashkurgan Valley, northwest Tibetan Plateau. *Quaternary Science Reviews*, 80: 91–101.

Yang Jianqiang, Zhang Wei, Cui Zhijiu, Yi Chaolu, Liu Kexin, Ju Yuanjiang and Zhang Xiaoyong, 2006. Late Pleistocene glaciation of the Diancang and Gongwang Mountains, southeast margin of the Tibetan Plateau. *Quaternary International*, 154/155: 52–62.

Yao Tandong and Thompson, L.G., 1992. Dundre Ice Core records temperature changes over the past 5 ka. *Science in China* (Series B), 22(10): 83–87 (in Chinese).

Yao Tandong, Chen Fahu, Cui Peng, Ma Yaoming, Xu Baiqing, Zhu Liping, Zhang Fan, Wang Weicai, Ai Likun and Yang Xiaoxin, 2017. From Tibetan Plateau to Third Pole and Pan-Third Pole. *Bulletin of Chinese Academy of Sciences*, 32(9): 924–931 (in Chinese with English abstract).

Yao Tandong, Thompson, L.G., Shi Yafeng, Qin Dahe, Jiao Keqin, Yang Zhihong, Tian Lide and Mosley-Thompson, E., 1997. Climate variation since the last interglaciation recorded in the Guliya ice core. *Science in China* (Series D), 27(5):447–452 (in Chinese).

Yi Chaolu, Chen Hualiang, Yang Jianqiang, Liu Bin, Fu Ping, Liu Kexin and Li Shijie, 2010. Review of holocene glacial chronologies based on radiocarbon dating in Tibet and its surrounding mountains. *Journal of Quaternary Science*, 23 (6/7): 533–543.

Yonker, C.M., Schimel, D.S., and Paroussis, E., 1998. Patterns of organic carbon accumulation in a semiarid shortgrass steppe, Colorado. *Soil Science Society of America Journal*, 52 (2): 478–483.

Zech, R., Abramowski, U., Glaser, B., Sosin, P., Kubik, P.W., and Zech, W., 2005a. Late Quaternary glacier and climate history of the Pamir Mountains derived from cosmogenic ^{10}Be exposure ages. *Quaternary Research*, 64(2): 212–220.

Zech, R., Glaser, B., Sosin, P., Kubik, P.W., and Zech, W., 2005b. Evidence for long-lasting landform surface instability on hummocky moraines in the Pamir Mountains (Tajikistan) from ^{10}Be surface exposure dating. *Earth & Planetary Science Letters*, 237(3): 453–461.

Zech, R., Zech, M., Kubik, P.W., Kharki, K., and Zech, W., 2009. Deglaciation and landscape history around Annapurna, Nepal, based on ^{10}Be surface exposure dating. *Quaternary Science Reviews*, 28(11/12): 1106–1118.

Zhang Yongshuang, Yao Xin, Yu Kai, Du Guoliang and Guo Changbao. 2016. Late-Quaternary slip rate and seismic activity of the Xianshuihe fault zone in southwest China. *Acta Geologica Sinica* (English Edition), 90(2): 525–536.

Zhang Zhigang, Wang Jian, Bai Shibiao, Xu Xiaobin and Chang Zhiyang, 2014a. Impact of surface rock erosion rate on in-situ cosmogenic exposure dating method. *Scientia Geographica Sinica*, 34(1): 116–121 (in Chinese with English abstract).

Zhang Zhigang, Xu Xiaobin, Wang Jian, Bai Shibiao and Chang Zhiyang, 2014b. Discussion of existing problems on the terrestrial cosmogenic nuclides exposure ages of Tibetan Plateau. *Geological Review*, 60(6): 1359–1369 (in Chinese with English abstract).

Zhang Zhigang, Xu Xiaobin, Wang Jian, Zhao Zhijun, Bai Shibiao and Chang Zhiyang, 2014c. Last deglaciation climatic fluctuation record by the Palaeo-Daocheng ice cap, southeastern Qinghai-Tibetan Plateau. *Acta Geologica Sinica* (English Edition), 88(6): 1863–1874.

Zhang Zhigang, Wang Jian, Xu Xiaobin, Bai Shibiao and Chang Zhiyang, 2015. Cosmogenic ^{10}Be and ^{26}Al chronology of the last glaciation of the Palaeo-Daocheng ice cap, southeastern Qinghai-Tibetan Plateau. *Acta Geologica Sinica* (English Edition), 89(2): 575–584.

Zhao Jingdong, Wang Jie and Shangguan Donghui, 2009. Sequences of the Quaternary glacial sediments and their preparatory chronology in the Tumur River valley, Tianshan Mountains. *Journal of Glaciology and Geocryology*, 31(4): 628–633 (in Chinese with English abstract).

Zhao Jingdong, Shi Yafeng and Wang Jie, 2011. Comparison

between Quaternary Glaciations in China and the Marine Oxygen Isotope Stage (MIS): An Improved Schema. *Acta Geographica Sinic*a, 66(7): 867–884 (in Chinese with English abstract).

Zhao Jingdong, Wang Jie and Yin Xiufeng, 2013. Quaternary Glaciations Research in China: Current Status and Controversy. *Journal of Glaciology and Geocryology*, 35(1): 119–125 (in Chinese with English abstract).

Zheng Du and Yao Tandong, 2004. Progress in research on formation and evolution of Tibetan Plateau with its environment and resource effects. *China Basic Science*, 6(2): 17–23 (in Chinese with English abstract).

Zhou Shangzhe and Li Jijun, 2003. New dating results of Quaternary glaciations in China. *Journal of Glaciology and Geocryology*, 25(6): 660–606 (in Chinese with English abstract).

Zhou Shangzhe, Xu Liubing, Cui Jianxin, Zhang Xiaowei and Zhao Jingdong. 2005. Geomorphologic evolution and environmental changes in the Shaluli Mountain region during the Quaternary. *Chinese Science Bulletin*, 50(1): 52–57.

Zhou Shangzhe, Wang Jie, Xu Liubing, Colgan, P.M., and Mickelson, D.M., 2010. Glacial advances in southeastern Tibet during late Quaternary and their implications for climatic changes. *Quaternary International*, 218(1/2): 58–66.

Zhou Shangzhe, Xu Liubing, Colgan, P.M., Mickelson, D.M., Wang Xiaoli, Wang Jie and Zhong Wei, 2007. Cosmogenic ^{10}Be dating of Guxiang and Baiyu glaciations. *Chinese Science Bulletin*, 52(1): 1387–1393.

About the first author

ZHANG Mengyuan, female; born in 1994 in Chengdu City, Sichuan Province; Postgraduate; She is now studying at Nanjing Normal University, and is now interested in the study on terrestrial cosmogenic nuclides exposure dating of glacier landforms. Email: 467027282@qq.com.